Materials Horizons

ROYAL SOCIETY OF CHEMISTRY

COMMUNICATION

View Article Online
View Journal | View Issue

Cite this: *Mater. Horiz.*, 2021, **8**, 1216

Received 29th December 2020,
Accepted 18th January 2021

DOI: 10.1039/d0mh02058c

rsc.li/materials-horizons

Cancer-microenvironment triggered self-assembling therapy with molecular blocks†

Hirotaka Nakatsuji,[a] Yudai Shioji,[b] Noboru Hiraoka,[b] Yuta Okada,[b] Natsuko Kato,[b] Sayaka Shibata,[c] Ichio Aoki[c] and Michiya Matsusaki *[ab]

Drug delivery systems (DDS) have been studied in an effort to reduce side effects by increasing the accumulation of anticancer drugs in cancer cells. However, the transport efficiency is still low due to the blocking by surrounding stromal tissues and the multiple intracellular drug transportation processes required to get the drug to a target cytosol. Thus, improving the efficiency of cancer therapy is still a major challenge. Here, a drug-free cancer microenvironment-targeting therapy using molecular blocks (MBs) is demonstrated, which is designed for efficient blood circulation and penetration through the stromal tissues as either a single molecule or a few molecules. When the MBs moved to a cancer microenvironment by the enhanced permeability and retention effect, they formed a self-assembled aggregate on the cancer cell surfaces in response to the weak acid (pH ~ 6.5) condition leading to subsequent cancer cell death by membrane disruption. This strategy avoids multiple intracellular transportation processes and also stimulates cell membrane disruption by self-assembly of the MB *via* hydrophobic interactions. Deoxycholic acid (DCA) was selected as a cancer microenvironment-responsive unit because its pK_a = 6.6. The DCA conjugated 4-arm poly(ethylene glycol) (4-MB) showed self-assembly phenomena on cancer cell membranes and subsequently significant cytotoxicity was clearly observed. Moreover, they clearly showed efficient accumulation in the tumor and the effective suppression of tumor growth in *in vivo* experiments. This MB therapy will be a new strategy for addressing the current issues of DDS.

New concepts

Recently, aggregation of molecules on cancer cell surfaces was reported as a novel mechanism for drug-free cancer pharmacotherapy which could avoid the problems of conventional antibody drugs and molecule targeted drugs, such as drug resistant cancers and limitation of coverage. However, it is difficult to avoid eliminating aggregates from blood vessels and non-specific accumulation causes side effects. Therefore, in this paper, a new concept of cancer pharmacotherapy using "molecular blocks" is demonstrated. The blocks were designed to disperse as nano-scale particles in blood vessels to avoid elimination and this enhances transport efficiency to the cancer tumor, and then they form micro-scale aggregates at the cancer tumor by self-assembling in response to the cancer microenvironment and are then retained and induce cancer cell death. A multi-arm poly(ethylene glycol) modified with deoxycholic acid which has a suitable pK_a to detect the weak acidic environment around the cancer tumor was utilized. A pH-dependent size change and cell killing ability of molecular blocks which occurred only in weakly acidic conditions was confirmed. Furthermore, they showed an efficient tumor accumulation property and a suppression effect on the tumor growth in animal experiments. These data demonstrated a proof-of-concept of "molecular blocks" as a novel strategy for cancer pharmacotherapy.

Chemotherapy is one of the effective modalities of cancer treatment but the severe adverse effects of anti-cancer drugs due to off-target cytotoxicity are still a problem. To overcome this problem, DDS which increase accumulation of an anti-cancer drug in cancer tissue and prolong circulation time have been widely developed and are already used clinically to avoid severe adverse effects and enhance the therapeutic effect. In particular, macromolecules containing polymers and nano-particles have been actively used as drug delivery carriers of anti-cancer drugs because of the advantages of prolonged blood circulation time and tumor accumulation properties due to the enhanced permeability and retention (EPR) effect.[1] However, the median delivery efficiency to the tumor of the reported DDS carriers is still 0.7%.[2,3] Moreover, the delivery of DDS carriers with an active targeting ligand to the target cancer cells in a tumor has been reported to be only 0.0014%.[4] In addition, further intra cellular delivery to the target location, such as the nucleus, decreases total delivery efficiency.[5] Molecular targeted therapy is one of the strategies for reducing off-target harmful effects. In particular, cell surface targeted therapies using antibodies or receptor ligands can overcome the limitation of

[a] *Joint Research Laboratory (TOPPAN) for Advanced Cell Regulatory Chemistry, 2-1 Yamadaoka, Suita city, Osaka, 565-0871, Japan*
E-mail: m-matsus@chem.eng.osaka-u.ac.jp
[b] *Division of Applied Chemistry, Osaka University Graduate School of Engineering, 2-1 Yamadaoka, Suita city, Osaka, 565-0871, Japan*
[c] *National Institute for Quantum and Radiological Science and Technology, 4-9-1 Anagawa Inage, Chiba city, Chiba, Japan*

† Electronic supplementary information (ESI) available. See DOI: 10.1039/d0mh02058c

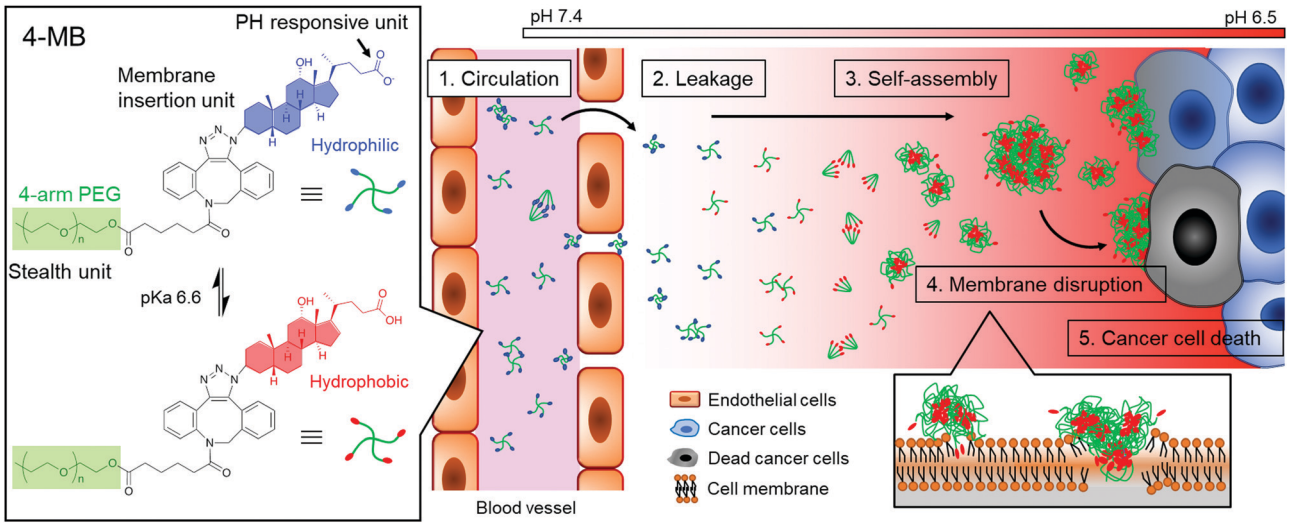

Fig. 1 Schematic illustration of a cancer microenvironment targeted therapy. Self-assembling of MBs and induction of cancer cell death response to the weak acidic conditions of the cancer tissue.

the intracellular transportation process. However, it also has drawbacks including high production costs, limited targets and weakness against drug-resistant cancers.[6] Therefore, drug-free therapeutics have been focused on recently, to address these issues. For example, a water-soluble polymer modified with antibody fragments has been reported to enhance apoptosis in malignant B cells by crosslinking the targeted surface receptors.[7–9] However, because antibody fragments are necessary for specific interaction to the target receptors, it has the same issue as the molecular targeted therapy.

Herein, a cancer microenvironment-targeting therapy is demonstrated, which uses molecular blocks (MBs) (Fig. 1). The MB is designed to exhibit the following three important characteristics: (1) blood circulation as a small particle, (2) self-assembly in response to a cancer microenvironment, and (3) cell membrane disruption. For the first characteristic, circulation in the blood as a single molecule or a few molecules is suitable for blood retention and accumulation properties in the tumor.[10] It is well known that nanoparticles ranging from a few nanometers to less than 100–200 nm have the ability to localize around cancer tissues and smaller particle sizes in that range have a higher transportation efficiency.[10]

For the second characteristic, the self-assembling property at the cancer cell membrane will be useful for enhancing retention effect in cancer tissue because a larger-sized particle can avoid clearance from the cancer tissue. Therefore, size-enlargement due to self-assembly would effectively enhance the accumulation efficiency.

For the third characteristic, the self-assembling property will also induce cancer cell death by disrupting the membrane *via* hydrophobic interaction. It was reported that self-assembly of peptides or macromolecules on cancer tissue induced cancer cell death[7–9,11,12] and inhibited cancer metastasis.[13] It is also expected that the membrane disruptive mechanism would be applicable to any type of cancer cells, even drug-resistant cancers, because of the simple physical effects.[14,15] Overall, cancer microenvironment-targeting therapy using MBs could overcome the issues of using conventional pharmacotherapy.

For the responsiveness to the cancer microenvironment, a weak acidic condition due to anaerobic respiration was focused on.[16,17] The DCA, which is one of the bile acids, was selected as a cancer microenvironment-responsive unit because of its acidity constant (pK_a) of 6.6. The DCA was expected to show self-assembling properties at the cancer microenvironment because of the hydrophobic interaction *via* protonation of carboxylate groups. In preliminary experiments, the DCA solution was significantly more viscous in weak acid conditions (pH 6.0) than in neutral conditions (pH 7.0) (Fig. S1, ESI†).

In this study, the DCA unit was conjugated to the end group of a multi-arm poly(ethylene glycol) (PEG) because it has been widely used as a biocompatible polymer with stealth properties to reduce antigenicity and prolong blood circulation time.[18] The DCA-conjugated multi-arm PEG was named as MB, which act as "*in vivo* blocks" to find and kill cancer cells.

The MBs were synthesized as shown in Scheme S1 (ESI†). The 3β-azidodeoxycholic acid was synthesized according to a previously reported method[19] and modification of the multi-arm PEG with DCA was performed by a copper-free click reaction. The MBs with 2, 4, and 8 arms of 5k PEG chain (2-MB10k, 4-MB20k and 8-MB40k) were successfully prepared, as confirmed by ^{1}H-NMR and IR spectroscopy (Fig. S2–S6, ESI†). To evaluate the dispersion property, static light scattering (SLS) and dynamic light scattering (DLS) measurements were performed on each of the MBs in phosphate-buffered saline (PBS) at pH 7.4 (Table S1, ESI†). The SLS data showed that only 8-MB40k was dispersed as a single molecule in neutral conditions and that 4-MB20k had the smallest particle size of approximately 50 nm by assembling nine molecules. This would suggest that the higher concentration of PEG in 8-MB40k causes a linear conformation of the polymer chain[18,20] compared to the other multi-arm PEGs. An MB with a lower molecular weight of 4-MB (4-MB10k) was also synthesized and it was expected to have a

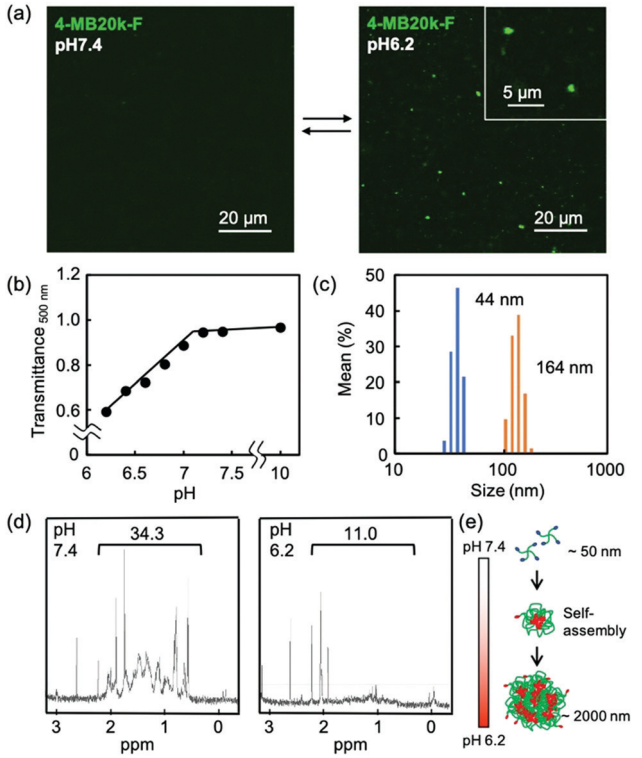

Fig. 2 (a) Fluorescence images of 4-MB20k-F (FITC) at 1 mg mL^{-1} at pH 7.4 and pH 6.2. (b) The pH-dependent transmittance changes of 4-MB20k solution. (c) Size distribution of 4-MB20k at 1 mg mL^{-1} at pH 6.2 (orange) and 7.4 (blue) evaluated by dynamic light scattering measurements. (d) The NMR spectra of 4-MBs in D_2O at pH 7.4 and pH 6.2 and integration of the DCA-derived peaks. (e) Schematic depiction of the self-assembly of MBs in response to a weak acidic condition.

smaller particle size. However, 4-MB10k showed a bigger particle size and wider size distribution than 4-MB20k, possibly because the decreased hydrophilic unit was not sufficient for stable dispersion. The critical micelle concentration (CMC) of MB solutions was evaluated using the pyrene method[21] and the results did not show a big difference (Fig. S7, ESI†). From these data, it was decided to use 4-MB20k for the subsequent cell experiments because they had the smallest particle size for blood circulation.

The self-assembling properties of MBs in a weak acid condition were confirmed by fluorescence microscopy using fluorescein labeled 4-MB20k (4-MB20k-F). The 4-MB20k-F showed aggregation of approximately 2 μm at pH 6.2 whereas there was no aggregation at pH 7.4 (Fig. 2a and Fig. S8, ESI†). Transmittance of the 4-MB20k solution decreased with a decreasing solution pH, suggesting the same aggregation manner occurred (Fig. 2b). The size distribution of MBs at pH 6.2 clearly showed aggregation formation with a size of 164 nm (Fig. 2c). Whereas a micro scale aggregate is out of the range of DLS measurement, a sub-micro scale aggregate was only found in this condition although a turbidity increase was clearly observed. To investigate the structural change of MBs, ^{1}H-NMR spectra in D_2O at pH 6.2 and 7.4 were measured. Interestingly, the peaks at 0.5 to 2.0 ppm assigned to DCA were clearly found in the neutral condition, but completely disappeared at pH 6.2, suggesting that the mobility of DCA was restricted by self-assembly caused by the hydrophobic interaction in a weak acidic condition due to the protonation of carboxylate groups (Fig. 2d and Fig. S9, ESI†). From these data, the prospective self-assembling process in an acidic condition is as follows: the MBs form submicron sized aggregates due to the hydrophobicity of DCA and the subsequent aggregation occurred because of the assembly of the sub-micron aggregate to form a larger aggregate of approximately 2 μm (Fig. 2e).

To clarify the adsorption property and cytotoxicity of MBs, 4-MB20k-F was incubated with cancer cells (Fig. 3a). A sample of 1 mg mL^{-1} of 4-MB20k-F in a culture medium at pH 7.4 or 6.2 were administered to human colon cancer cells (HT-29) and time course images were observed by confocal laser scanning microscopy (CLSM). The 4-MB20k-F accumulated on the cell surface and subsequent cell detachment was observed only at pH 6.2 after 24 h incubation (Fig. 3b and c, and Movie S1, ESI†). At the same time, they showed significantly higher cytotoxicity at pH 6.2 than at pH 7.4 with concentrations of 4-MB20k-F greater than 0.5 mg mL^{-1} condition (Fig. 3d and Fig. S10a, S11, ESI†). It was confirmed that the DCA unit is necessary for this phenomenon by comparison to the results obtained with 4-PEG20k (Fig. S10b, ESI†). Interestingly, the cell killing property was also found to occur not only in other types of human cancer cells, such as cervical cancer (HeLa), lung cancer (A549), and pancreatic cancer (MIA PaCa-2), but also in normal cells (normal human dermal fibroblast: NHDF) in a weak acidic condition because the mechanism is simple cell membrane disruption due to the hydrophobic interaction between protonated DCA and the lipid membrane (Fig. 3e and Fig. S12, ESI†) and it is non-selective for cancer cells. However, because a weak acidic condition generally only occurred at the cancer microenvironments due to anaerobic respiration,[16,17] normal tissue should not incur heavy damage from the MBs. In other words, cancer cells in an anaerobic condition in solid tumors will suffer similar amounts of damage from MBs independent of cancer cell type. This is a notable benefit of MBs as a universal treatment independent of genetic heterogeneity between and within tumors.[22] In addition, the reversible self-assembling property (Fig. 2a) would avoid any harmful effects of residual MBs after cancer treatment.

The mechanism of cytotoxicity was investigated by flow cytometry and CLSM imaging using an apoptotic/necrotic/healthy cells detection kit (Fig. 3f, g and Fig. S13, ESI†). The 96% of the dead cells were from necrosis caused by accumulation of MBs on the cell surface.

Because the insertion of a cholesteric unit of DCA into the cell membrane by hydrophobic interaction has been reported,[14,23] the necrosis found in this study would appear to be due to the accumulation of MBs in the membrane. The therapeutic effects of MBs on cancer tissue were also evaluated using a three dimensional (3D) cancer model because two dimensional (2D) cultured cancer cells sometimes show a different drug response from *in vivo* animal models because they do not have the surrounding stromal tissue.[24] A novel sedimentary culture method to construct stromal tissue with

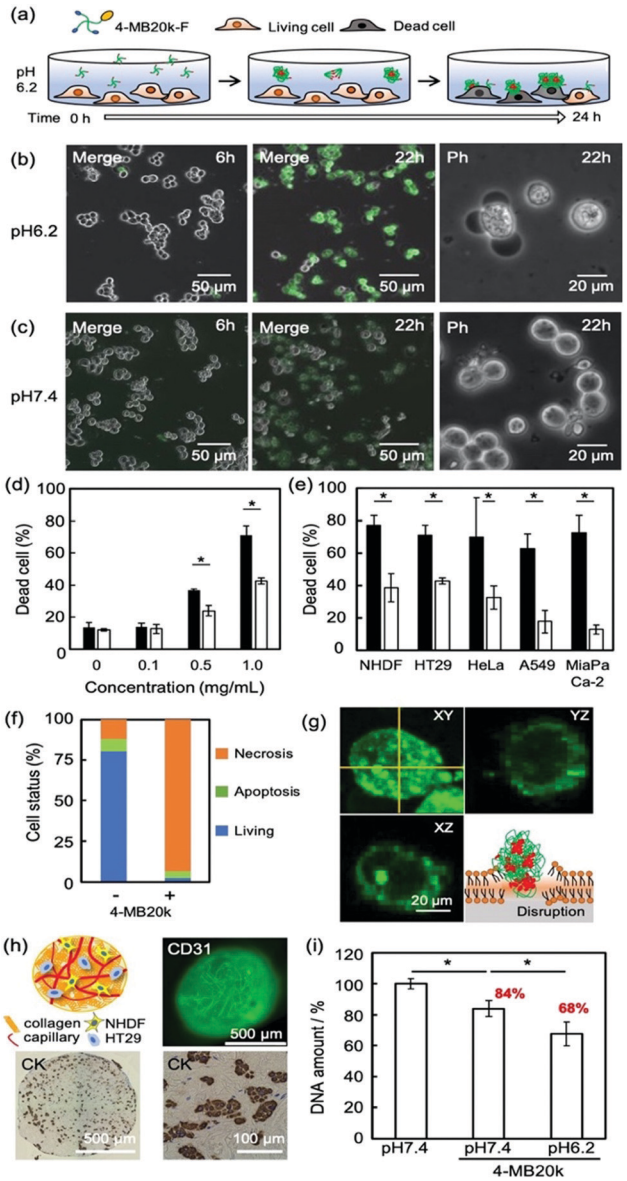

Fig. 3 (a) Evaluation procedure of the adsorption and cell killing ability of 4-MB-F. Time lapse fluorescence images of cancer cells (HT-29) treated with 4-MB20k-F at pH 6.2 (b) and at pH 7.4 (c). The right-hand side images are high magnification phase (Ph) contrast images taken after 24 h after treatment. (d) Concentration-dependent cell-killing ability of 4-MB20k at pH 6.2 (closed) and 7.4 (open) (n = 3). (e) Cell killing activity of 4-MB20k at 1 mg mL^{-1} against NHDF, HT-29, HeLa, A549 and MiaPaCa-2 at pH 6.2 (closed) and 7.4 (open) (n = 3). (f) Percentage of living, early apoptotic and necrotic stages of HT-29 cells after treatment with 4-MB20k. (g) 3D reconstructed CLSM images of HT-29 treated with 4-MB20k-F for 24 h. Illustration is the disruption of the cell membrane induced by self-assembly of the MBs. (h) Illustration of 3D tumor models including stroma (top left) and CLSM images of GFP HUVEC networks in the 3D tumor models (top right). The lower (bottom left) and higher (bottom right) magnification immunostaining images of the 3D tumor models by cytokeratin (CK). The brown colored cells are HT-29 cells. (i) The amount of DNA in the 3D tumor models after treatment with MBs under both pH conditions. The p-value was evaluated by Student's t-test. *p <0.05, (n = 3).

high density collagens, fibroblasts, and blood capillary networks using collagen microfibers was recently reported.[25,26] The 3D cancer models constructed indicated embedded HT-29 colonies surrounded by high density collagen fibers with fibroblasts and blood capillaries (Fig. 3h and Fig. S14, ESI†), suggesting that it may have cancer microenvironments similar to those found in *in vivo* animal models. After the treatment of the 3D cancer models with 4-MB20k at pH 7.4 in the same manner as the 2D models as shown in Fig. 3a, the remaining living cell number decreased to 84%, suggesting the existence of a weak acid cancer microenvironment in the 3D stromal tissues (Fig. 3i). Moreover, the living cell number dropped further to 68% after 4-MB20k treatment at pH 6.2 because of the higher self-assembling property of 4-MB20k to disrupt the cancer cell membrane. The results of 2D and 3D models clearly demonstrated the possibility of using the 4-MBs for microenvironment-targeted cancer therapy.

Finally, the *in vivo* localization property and the therapeutic effect of 4-MBs was evaluated by intravenous (iv) administration of the near-infrared fluorescence dye (Cy5.5) labeled 4-MB20k (4-MB20k-C) to tumor-bearing mice (Fig. 4a). The fluorescence intensity of 4-MB20k-C at the tumor region gradually increased for 24 h, whereas the fluorescence intensity in the liver region gradually decreased, which suggests a longer blood half-life than that of commercial chemotherapy drugs such as 5-FU (blood half-life is 8–22 min[27]) (Fig. 4b and Fig. S15, ESI†). The fluorescence intensity of 4-MB20k-C at the tumor region was approximately five times higher than that of the surrounding muscles (Fig. 4c and Fig. S16, ESI†) which might be due to the high blood circulation of the small particle size (<50 nm) 4-MB20k-C, because of minimal molecular assembly (Fig. 2c). The transportation efficiency to the tumor was estimated to be 1.4% by collecting 4-MB20k-C from the homogenized tumor solutions, suggesting a two-fold higher transportation efficiency than that of the median value (0.7%) of the reported meta-analysis[2,4] (Fig. 4d). Surprisingly, although the targeting mechanism of 4-MB20k-C was the passive EPR effect, it indicated a higher transportation efficiency than that of the average value of active targeting (0.9%).[2,3] The results clearly demonstrated the possibility of using cancer microenvironment targeting therapy using 4-MBs as a new therapy. However, a limitation of using the current 4-MBs structures was also found, which was because of higher accumulations found in the liver, kidney and spleen regions (Fig. 4e and Fig. S16, ESI†). This may be due to the hydrophobicity of the dibenzyl cyclooctyne (DBCO) unit which was used in the copper-free click reaction.[28] If the DBCO-free MBs are synthesized in the future, the accumulation issues in the organs will need to be addressed and subsequent transportation efficiency to target tumors should be improved. Although the delivery efficiency of the 4-MB20k-C was only 1.4%, a suppression effect of tumor growth was clearly found after 12 d of administration without significant body weight change (Fig. 4f and Fig. S16, ESI†). The localization of the 4-MB20k-C was also confirmed by histological analyses with hematoxylin and eosin (H&E) staining, Azan staining, and immunostaining of CD31 (Fig. 4g, h and Fig. S17, ESI†). The MBs were mainly accumulated around the blood vessels indicated by the arrows and in the interface between the cancer cells and the stroma. These data supported the

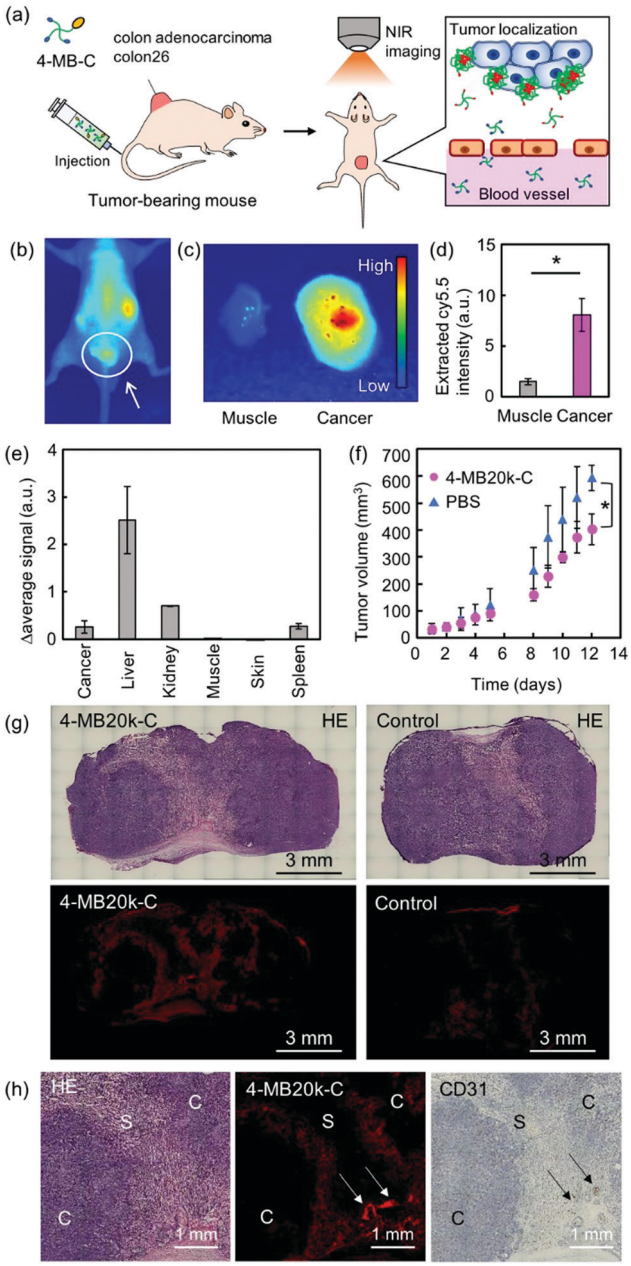

Fig. 4 (a) Evaluation of tumor localization effect and therapeutic effect of 4-MB20k-C (Cy5.5) using tumor bearing mouse. (b) *In vivo* fluorescence image of a tumor bearing mouse 24 h after injection of 4 mg of 4-MB20k-C. The white circle indicates the tumor regions. (c) Fluorescence *ex vivo* image of the tumor and surrounding muscle extracted from the tumor bearing mouse, and (d) fluorescence intensity of 4-MB20k-C extracted from each tissue (n = 3). (e) Δfluorescence signals from each organ extracted from a MB or a PBS treated mouse (n = 3). (f) Time course image of the tumor volume of the mice. PBS (10 μl g^{-1}) or 4-MB20k-C (0.075 mg mL^{-1}) in PBS were injected into the mice per day. (g) Histological analyses of tissues, from injected mice, with H&E staining (top) and fluorescence staining (bottom) images of the extracted tumor from 4-MB20k-C (left) and PBS (right). (h) High magnification images of H&E and fluorescence staining, and CD31 antibody immunostaining of a 4-MB20k-C treated tumor (g). Arrows indicate blood vessels. C and S indicate cancer cells and stroma, respectively. The p-value was evaluated by Student's t-test. * $p < 0.05$, (n = 2–3).

mechanism where MBs have leaked from blood vessels and accumulated in response to the tumor microenvironment without accumulating in the stroma. In addition, histological analyses were also performed with H&E staining and immunostaining of CD3 and F4/80 for the extracted organs from MB injected mice to evaluate their biocompatibility. The MBs have not yet shown severe damage in the organs (Fig. S18 and S19, ESI†). In addition, the number of immunostained T-cells (CD3, Fig. S20 and S21, ESI†) and macrophages (F4/80, Fig. S22 and S23, ESI†) have not shown a significant difference, when injected with PBS (control), which strongly suggested that MBs had not induced significant inflammation in the organs. These data clearly suggest that 4-MBs have great potential as a new type of drug-free cancer therapy.

Conclusions

In summary, a new drug-free approach to cancer treatment was demonstrated using cancer microenvironment targeted therapy with MBs composed of PEG and DCA possessing pK_a = 6.6 similar to the weak acid conditions of a tumor. The MBs were designed to exhibit three important characteristics: circulation in the blood as a small particle, self-assembly in response to a cancer microenvironment, and cell membrane disruption. The 4-MB20k indicated a self-assembling property in weak acid conditions and aggregated to form a micrometer-sized particle. Although the transportation efficiency of 4-MBs to the tumor was two-fold higher than that of the median value of the reported meta-analysis, a limitation of the current 4-MBs structures was also observed because of higher accumulations found in the liver, kidney and spleen regions. Improvements in efficiency will be realized by modification of the chemical structure of 4-MBs to avoid the use of hydrophobic DBCO. However, the MBs showed a suppression effect of tumor growth without significantly severe damage and inflammation of major organs. The use of the MBs is expected to create new opportunities in cancer microenvironment targeting therapy for cancer treatment.

Conflicts of interest

The authors declare no competing financial interest.

Acknowledgements

The authors thank Nippon Ham Foods, Ltd, for their kind donation of type I collagen. This research was supported by the Grant-in-Aid for Scientific Research (A) (20H00665), the Bilateral Joint Research Projects of the JSPS, and the AMED Grants (JP18be0304207, 19lm0203014j0001).

Notes and references

1 Y. Matsumura and H. Maeda, *Cancer Res.*, 1986, **46**, 6387–6392.

2 S. Wilhelm, A. J. Tavares, Q. Dai, S. Ohta, J. Audet, H. F. Dvorak and W. C. W. Chan, *Nat. Rev. Mater.*, 2016, **1**, 1–12.
3 M. Torrice, *ACS Cent. Sci.*, 2016, **2**, 434–437.
4 Q. Dai, S. Wilhelm, D. Ding, A. M. Syed, S. Sindhwani, Y. Zhang, Y. Y. Chen, P. MacMillan and W. C. W. Chan, *ACS Nano*, 2018, 8423.
5 M. E. Davis, Z. G. Chen and D. M. Shin, *Nat. Rev. Drug Discovery*, 2008, **7**, 771–782.
6 Y. T. Lee, Y. J. Tan and C. E. Oon, *Eur. J. Pharmacol.*, 2018, **834**, 188–196.
7 T. W. Chu and J. Kopecek, *Biomater. Sci.*, 2015, **3**, 908–922.
8 L. Li, J. Yang, J. Wang and J. Kopecek, *Macromol. Biosci.*, 2018, **18**, 1700196.
9 K. Wu, J. Liu, R. N. Johnson, J. Yang and J. Kopecek, *Angew. Chem., Int. Ed.*, 2010, **49**, 1451–1455.
10 Y. Matsumoto, J. W. Nichols, K. Toh, T. Nomoto, H. Cabral, Y. Miura, R. J. Christie, N. Yamada, T. Ogura, M. R. Kano, Y. Matsumura, N. Nishiyama, T. Yamasoba, Y. H. Bae and K. Kataoka, *Nat. Nanotechnol.*, 2016, **11**, 533–538.
11 J. Zhou, X. Du, N. Yamagata and B. Xu, *J. Am. Chem. Soc.*, 2016, **138**, 3813–3823.
12 Y. Kuang, J. Shi, J. Li, D. Yuan, K. A. Alberti, Q. Xu and B. Xu, *Angew. Chem., Int. Ed.*, 2014, **53**, 8104–8107.
13 X. X. Hu, P. P. He, G. B. Qi, Y. J. Gao, Y. X. Lin, C. Yang, P. P. Yang, H. Hao, L. Wang and H. Wang, *ACS Nano*, 2017, **11**, 4086–4096.
14 N. H. Park, W. Cheng, F. Lai, C. Yang, P. Florez de Sessions, B. Periaswamy, C. W. Chu, S. Bianco, S. Liu, S. Venkataraman, Q. Chen, Y. Y. Yang and J. L. Hedrick, *J. Am. Chem. Soc.*, 2018, **140**, 4244–4252.
15 F. Fan, J. G. Piao, Y. Zhao, L. Jin, M. Li, Y. Wang and L. Yang, *ACS Appl. Bio Mater.*, 2020, **3**, 1267–1275.
16 O. Warburg, *Science*, 1956, **123**, 309–314.
17 T. Ma, Y. Hou, J. Zeng, C. Liu, P. Zhang, L. Jing, D. Shangguan and M. Gao, *J. Am. Chem. Soc.*, 2018, **140**, 211–218.
18 J. S. Suk, Q. G. Xu, N. Kim, J. Hanes and L. M. Ensign, *Adv. Drug Delivery Rev.*, 2016, **99**, 28–51.
19 P. Verwilst, S. V. Eliseeva, S. Carron, L. Vander Elst, C. Burtea, G. Dehaen, S. Laurent, K. Binnemans, R. N. Muller, T. N. Parac-Vogt and W. M. De Borggraeve, *Eur. J. Inorg. Chem.*, 2011, 3577–3585.
20 Q. Yang, S. W. Jones, C. L. Parker, W. C. Zamboni, J. E. Bear and S. K. Lai, *Mol. Pharmaceutics*, 2014, **11**, 1250–1258.
21 M. Wilhelm, C. L. Zhao, Y. C. Wang, R. L. Xu, M. A. Winnik, J. L. Mura, G. Riess and M. D. Croucher, *Macromolecules*, 1991, **24**, 1033–1040.
22 R. A. Burrell, N. McGranahan, J. Bartek and C. Swanton, *Nature*, 2013, **501**, 338–345.
23 S. Jean-Louis, S. Akare, M. A. Ali, E. A. Mash, Jr., E. Meuillet and J. D. Martinez, *J. Biol. Chem.*, 2006, **281**, 14948–14986.
24 A. Nishiguchi, M. Matsusaki, M. R. Kano, H. Nishihara, D. Okano, Y. Asano, H. Shimoda, S. Kishimoto, S. Iwai and M. Akashi, *Biomaterials*, 2018, **179**, 144–155.
25 F. Louis, S. Kitano, J. F. Mano and M. Matsusaki, *Acta Biomater.*, 2019, **84**, 194–207.
26 Y. Naka, S. Kitano, S. Irie and M. Matsusaki, *Mater. Today Bio*, 2020, **6**, 100054.
27 R. B. Diasio and B. E. Harris, *Clin. Pharmacokinet.*, 1989, **16**, 215–237.
28 J. Jeon, J. A. Kang, H. E. Shim, Y. R. Nam, S. Yoon, H. R. Kim, D. E. Lee and S. H. Park, *Bioorg. Med. Chem.*, 2015, **23**, 3303–3308.